

Asparagine and Aspartate Hydroxylation of the Cytoskeletal Ankyrin Family Is Catalyzed by Factor-inhibiting Hypoxia-inducible Factor^{*[S]}

Received for publication, October 12, 2010, and in revised form, December 3, 2010. Published, JBC Papers in Press, December 22, 2010, DOI 10.1074/jbc.M110.193540

Ming Yang[‡], Wei Ge^{‡1}, Rasheduzzaman Chowdhury^{‡1}, Timothy D. W. Claridge^{‡1}, Holger B. Kramer[§], Bernhard Schmierer[¶], Michael A. McDonough[‡], Lingzhi Gong[‡], Benedikt M. Kessler[§], Peter J. Ratcliffe[§], Mathew L. Coleman^{§2}, and Christopher J. Schofield^{‡2,3}

From the [‡]Chemistry Research Laboratory and Oxford Centre for Integrative Systems Biology, University of Oxford, Oxford OX1 3TA, United Kingdom, the [¶]Department of Biochemistry and Oxford Centre for Integrative Systems Biology, University of Oxford, South Parks Road, Oxford OX1 3QU, and the [§]Henry Wellcome Building for Molecular Physiology, University of Oxford, Oxford OX3 7BN, United Kingdom

Factor-inhibiting hypoxia-inducible factor (FIH) catalyzes the β -hydroxylation of an asparagine residue in the C-terminal transcriptional activation domain of the hypoxia inducible factor (HIF), a modification that negatively regulates HIF transcriptional activity. FIH also catalyzes the hydroxylation of highly conserved Asn residues within the ubiquitous ankyrin repeat domain (ARD)-containing proteins. Hydroxylation has been shown to stabilize localized regions of the ARD fold in the case of a three-repeat consensus ankyrin protein, but this phenomenon has not been demonstrated for the extensive naturally occurring ARDs. Here we report that the cytoskeletal ankyrin family are substrates for FIH-catalyzed hydroxylations. We show that the ARD of ankyrinR is multiply hydroxylated by FIH both *in vitro* and in endogenous proteins purified from human and mouse erythrocytes. Hydroxylation of the D34 region of ankyrinR ARD (ankyrin repeats 13–24) increases its conformational stability and leads to a reduction in its interaction with the cytoplasmic domain of band 3 (CDB3), demonstrating the potential for FIH-catalyzed hydroxylation to modulate protein-protein interactions. Unexpectedly we found that aspartate residues in ankyrinR and ankyrinB are hydroxylated and that FIH-catalyzed aspartate hydroxylation also occurs in other naturally occurring AR sequences. The crystal structure of an FIH variant in complex with an Asp-substrate peptide together with NMR analyses of the hydroxylation product identifies the 3S regio- and stereoselectivity of the FIH-catalyzed Asp hydroxylation, revealing a previously unprecedented posttranslational modification.

Factor-inhibiting hypoxia-inducible factor (FIH)⁴ was originally identified as a negative regulator of the hypoxia inducible factor (HIF), a transcription factor that mediates the hypoxia response in animals (1). FIH-catalyzed hydroxylation of an asparagine (Asn) residue in the C-terminal transcriptional activation domain (CAD) of human HIF- α reduces the interaction between HIF and the transcriptional coactivator proteins p300/CBP (2), thereby reducing the expression of HIF-regulated genes. The dependence of FIH on oxygen for catalysis enables it to act as a sensor for hypoxia (3, 4). FIH not only catalyzes the β -hydroxylation of Asn residues in HIF- α isoforms but also of ankyrin repeat domain (ARD)-containing proteins (5–9) (supplemental Scheme 1). In contrast to its “switch-like” role in HIF regulation, the role(s) of Asn hydroxylation of the ubiquitous ARD proteins is unknown; it has been proposed that the extent of ARD hydroxylation regulates the amount of FIH available for HIF hydroxylation (6, 10).

The ankyrin repeat domain comprises a variable number of ~33 residue ankyrin repeats (ARs) that are arranged into a helix-loop-helix- β -hairpin/loop conformation (11). ARDs are predicted to be present in >300 proteins encoded by the human genome (12) and are involved in a range of processes including signaling, development, epigenetic regulation, and cellular structure (13, 14). To date most studies on FIH-catalyzed ARD hydroxylations have involved signaling proteins (5–9), where several Asn hydroxylation sites have been identified *in vivo*, with incomplete and widely varying levels of hydroxylation (5–96%) being observed (5, 6, 9). Proteomic (8) and biochemical analyses (5) suggest that ARD hydroxylation might be widespread.

Trans-Prolyl-4 hydroxylation of the extracellular matrix protein collagen occurs extensively in (Pro-Pro-Gly)_n motifs and stabilizes the collagen triple helix structure (15, 16). Crystallization studies on ARD proteins have shown that Asn hy-

* This work was funded by the Biotechnology and Biological Sciences Research Council, the European Union, the OAK Foundation, and the Wellcome Trust.

[S] The on-line version of this article (available at <http://www.jbc.org>) contains supplemental Schemes S1 and S2, Tables S1 and S2, and Figs. S1–S37.

⌘ Author's Choice—Final version full access.

The atomic coordinates and structure factors (code 2xum) have been deposited in the Protein Data Bank, Research Collaboratory for Structural Bioinformatics, Rutgers University, New Brunswick, NJ (<http://www.rcsb.org/>).

¹ These authors contributed equally to this work.

² Both authors contributed equally to this work.

³ To whom correspondence should be addressed: Chemistry Research Laboratory, University of Oxford, 12 Mansfield Rd., Oxford OX1 3TA, UK. Tel.: 44-1865-275625; Fax: 44-1865-275674; E-mail: christopher.schofield@chem.ox.ac.uk.

⁴ The abbreviations used are: FIH, factor inhibiting HIF; HIF, hypoxia-inducible factor; 2OG, 2-oxoglutarate; AR, ankyrin repeat; ARD, AR domain; CAD, C-terminal transactivation domain of HIF- α ; CDB3, cytoplasmic domain of band 3; DSC, differential scanning calorimetry; HSQC, heteronuclear single quantum coherence; IPAA, 5, 6-isopropylidene-L-ascorbic acid; TOCSY, total correlation spectroscopy; UPLC, ultra performance liquid chromatography; NOG, N-oxalylglycine; aa, amino acids.

droxylation does not alter the stereotypical ankyrin fold (6, 17). However, solution studies have revealed that Asn hydroxylation stabilizes consensus ARD proteins with respect to unfolding (17, 18). The question then arises as to whether ARD proteins that have a structural role in cells undergo Asn hydroxylation. The human cytoskeletal ankyrin family, which serve as adapters linking a variety of integral membrane proteins to the spectrin-cytoskeleton, includes three members: ankyrinR, ankyrinB, and ankyrinG (19). All three ankyrins contain 24 ARs in their membrane binding domains. Here we show that peptide fragments derived from ankyrinR, ankyrinB, and ankyrinG are substrates for FIH. We demonstrate that the ankyrinR ARD undergoes multiple FIH-catalyzed Asn hydroxylations both *in vitro* and *in vivo*. Hydroxylation of ankyrinR D34 causes its stabilization and may modulate its interaction with the cytoplasmic domain of band 3 (CDB3). Unexpectedly, we found that FIH catalyzes the aspartate (Asp) hydroxylation of ankyrinR and ankyrinB. Using biochemical assays, NMR, and crystallographic analyses, we show that FIH also hydroxylates Asp residues in other AR sequences to generate the novel 2S,3S-hydroxyaspartate product. Taken together the results expand the scope of FIH-catalyzed post-translational modifications.

EXPERIMENTAL PROCEDURES

Plasmid—pGEX-KG D34 (ankyrinR aa 402–827, ARs 13–24) was a kind gift from P. Michaely (University of Texas Southwestern Medical Center, Dallas, TX). pGEX-6p1-ankyrinB (ankyrinB aa 1–959, ARs 1–24) was a generous gift from V. Bennett (Duke University). pEF1/V5-HIS D34 was generated by PCR using pGEX-KG D34 as the template. pEF1/V5-HIS D12 (ankyrinR aa 1–402, ARs 1–12) was generated by PCR using human fetal cDNA as template. pFLAG-CMV2 CDB3 (aa 2–379) was generated by PCR using pET-21a CDB3 (kind gift from Z. Zhang, Fudan University) as the template. pET28a FIH, pCDNA3 FIH, and pCDNA3 FIH D201A plasmids were as described previously (6). The FIH Q239H mutant was generated by standard techniques. The integrity of all constructs was verified by sequencing.

Peptide Synthesis—Peptides used for *in vitro* incubation assays with FIH were prepared using an Intavis Multiprep automated peptide synthesizer using Tentagel-S-RAM resin (Rapp-Polymere) using standard 9-fluorenylmethoxycarbonyl/*N,N'*-diisopropylcarbodiimide/1-hydroxybenzotriazole strategy. Final cleavage using 2.5% triisopropylsilane in trifluoroacetic acid yielded the peptides as C-terminal amides that were precipitated in cold ether, re-dissolved in 0.1% trifluoroacetic acid in water, and lyophilized. The masses of the predicted peptide products were confirmed using a Micromass MALDI-TOF (Waters) mass spectrometer.

Recombinant Protein Expression and Purification—AnkyrinR D34 and the ankyrinB ARD were prepared by glutathione affinity and size exclusion chromatography to >90% purity using buffer containing 20 mM HEPES, pH 7.5, 500 mM NaBr, 2.5 mM CaCl₂ (Buffer A). D34-OH was prepared by co-expression of pGEX-KG D34 and pET-28a FIH in *Escherichia coli* BL21 (DE3). After induction with 0.5 mM isopropyl- β -D-thiogalactoside, the cells were supplemented with a

final concentration of 40 μ M Fe(II), 1.6 mM 2-oxoglutarate (2OG), and 1.2 mM 5,6-isopropylidene-L-ascorbic acid (IPAA) and were grown for 4 h before harvest. The cells were lysed by sonication in Buffer A supplemented with 40 μ M Fe(II), 5 mM 2OG, and 1.2 mM IPAA and incubated at room temperature for 1 h with stirring. Purification of D34-OH was as for the unhydroxylated material. CDB3 was prepared as described (20).

2OG Decarboxylation and *in Vitro* FIH Hydroxylations—Recombinant D34 was tested for the ability to stimulate FIH-dependent decarboxylation of ¹⁴C-labeled 2OG as described (3). *In vitro* FIH incubation assay used 20–60 μ M FIH, 100 μ M Fe(II), 100 μ M peptidyl substrate, 1 mM 2OG, and 1.2 mM IPAA. The assay mixtures were incubated at 37 °C for 30 min before analyses.

Cell Culture and Transfection—HEK293T cells were grown in Dulbecco's modified Eagle's medium supplemented with 10% fetal calf serum, 50 IU/ml penicillin, 50 μ g/ml streptomycin, and 2mM L-glutamine. Transfection was with FuGENE 6 (Roche Applied Science) according to the manufacturer's instructions.

Antibodies, Immunoprecipitation, and GST Pulldown Assays—Forty-eight hours after transfection cells were lysed in IP buffer (20 mM Tris-HCl, pH 7.4, 100 mM NaCl, 5 mM MgCl₂, 0.5% (v/v) Igepal CA-630, 1 \times Complete protease inhibitor mixture (Roche Applied Science)), and V5-D34 affinity purified using anti-V5 antibody resin (Sigma). Immuno-complexes were washed 3 times in IP buffer before elution in 2 \times Laemmli buffer and separation by SDS-PAGE. Immunoblots were performed using the following HRP-conjugated antibodies at a dilution of 1:5000: anti-HA (Roche Applied Science), anti-V5 (AbD Serotec), and anti-FLAG (Sigma). GST pulldown assays were performed as described (21).

Purification of Endogenous AnkyrinR—Human blood samples used in this study were provided by a healthy laboratory donor following written informed consent with ethical approval from the Mid and South Buckinghamshire Research Ethics Committee (REC reference 08/H0607/50). Endogenous ankyrinR was essentially purified from 50 ml of freshly drawn human blood as described (22). SDS-PAGE gel bands corresponding to the correct size of ankyrinR were excised and subjected to trypsin or endoproteinase GluC digestion followed by MS analyses. Mouse endogenous ankyrinR was purified following the same protocol except that 5 ml of blood was isolated from four mice by cardiac puncture.

Mass Spectrometry—Coomassie Blue-stained protein-containing bands were excised and digested with either trypsin (Promega) or endoproteinase GluC (Roche Applied Science) essentially as described (8). The resultant digest mixtures were analyzed by nano-ultraperformance liquid chromatography tandem mass spectrometry (nanoUPLC-MS/MS) using a 75- μ m inner diameter, 25-cm length C18 nano-AcquityTM UPLCTM column (1.7 μ m particle size; Waters) and a 90-min gradient of 2–45% solvent B (solvent A: 99.9% H₂O, 0.1% formic acid; solvent B: 99.9% acetonitrile, 0.1% formic acid) on a Waters nanoAcquity UPLC system (final flow rate 250 nl/min; 6000–7000 p.s.i.) coupled to a Q-TOF (quadrupole time-of-flight) Premier tandem mass spectrometer (Waters). MS

Ankyrin Asparagine and Aspartate Hydroxylation by FIH

analyses were performed in data-directed analysis mode (MS to MS/MS switching at precursor ion counts greater than 10 and MS/MS collision energy dependent on precursor ion mass and charge state). Raw MS data were processed with ProteinLynx Global Server software (PLGS Version 2.2.5) including de-isotoping. The mass accuracy of the raw data was calibrated using Glu-fibrinopeptide (200 fmol/ μ l; 700 nl/min flow rate; 785.8426 Da [$M+2H$] $^{2+}$) that was infused into the mass spectrometer as a lock mass during sample analysis. MS and MS/MS data were calibrated at intervals of 30 s. For the identification of endogenous ankyrinR, data-directed analysis-derived MS/MS spectra (peaklists) were searched against the UniprotKB/Swissprot data base (release 2010_07, 2010/06/18, 20,355 human sequences and 16,299 mouse sequences) using the Mascot algorithm (Version 2.2, Matrix Science) on an in-house server (The Computational Biology Research Group, University of Oxford) with the following parameters: peptide tolerance, 0.2 Da; $^{13}C = 1$; fragment tolerance, 0.1 Da; trypsin missed cleavages, 1; instrument type, electrospray ionization-quadrupole-TOF; variable modifications: M/N/D/HW oxidation, N/Q deamidation, no fixed modifications. The minimum threshold score/expect cut-off for accepting an individual MS/MS spectrum was $>45/0.013$, which assured the presence of at least 6–8 consecutive b or y ions covering the post-translationally modified residue. Assignments of hydroxylations that were detected by PLGS and Mascot were evaluated and verified by manual inspection. For quantitative comparison of non-hydroxylated *versus* hydroxylated peptide peaks, the sum of all MS spectra containing the relevant precursor ion pairs are shown, and the ratio was calculated by comparing the sum of ion counts for all isotopic peaks of the corresponding precursor ions.

MALDI-TOF MS analyses of synthetic peptides were performed on a Waters MicromassTM MALDI micro MXTM mass spectrometer in positive ion reflectron mode using α -cyano-4-hydroxycinnamic acid as the MALDI matrix. Instrument parameters used were: laser energy, 141%; pulse, 2050 V; detector, 2700V; suppression, 1500. The MALDI data were analyzed using MassLynxTM Version 4.1. MS/MS analyses of synthetic peptides was performed on a SynaptTM high definition mass spectrometryTM (Micromass Ltd) using a 2.1×100 -mm C18 Acquity UPLC[®] BEH300 column (1.7- μ m particle size; Waters) and a 4-min gradient of 5–50% solvent B at a flow rate of 0.4 ml/min. LC/MS was performed at trap CE 6V and transfer CE 4V, and MS/MS was performed at trap CE 35V and transfer CE 4V.

CD and Differential Scanning Calorimetry (DSC)

Analyses—CD experiments were performed using a Chirascan Circular Dichroism Spectrometer (Applied Photophysics) equipped with a Peltier temperature controller. The temperature inside the cuvette was recorded during the scan and used in the subsequent analyses. A cuvette with a path length 0.1 cm was used. For thermally induced unfolding, D34 samples were buffered in 1 mM Tris, 400 mM NaF, pH 7.4, at a protein concentration of 2.5 μ M. Thermal denaturation used stepped ramping at a rate of 1 $^{\circ}C \text{ min}^{-1}$, and the signal was averaged over 3 scans at each temperature. For equilibrium unfolding, aliquots of urea solutions were prepared by dispensing the

appropriate volumes of 10 M urea solution in buffer (1 mM Tris, 400 mM NaF, pH 7.4). Protein stock was then added to a final concentration of 2 μ M. Samples were incubated at 25 $^{\circ}C$ for 16 h before measurement. For native proteins (at 0 M urea), at least three spectra between 200 and 250 nm were recorded and averaged to determine whether the spectrum had the expected shape. At all other urea concentrations, the ellipticity at 222 nm was recorded, and three points were averaged. The denaturation curves were fitted to a three-state model described previously (23) using SigmaPlot. DSC scans were collected using a MicroCal VP DSC Microcalorimeter (MicroCal, Northampton, MA) at a protein concentration of 20 μ M in Buffer A at a scan rate of 1 $^{\circ}C \text{ min}^{-1}$.

NMR Analyses—The Asp-substrate peptide HLEVVKLLLEHGADVDAQDK was hydroxylated ($\sim 75\%$) by incubation with FIH in the presence of 2OG, Fe(II), and IPAA at 37 $^{\circ}C$ for 4 h. The reaction was quenched by the addition of trifluoroacetic acid (2%). Precipitated protein was removed by centrifugation, and the hydroxylated product was purified by HPLC using a Vydac 218TP C18 reversed phase column (250 \times 22 mm; particle size, 10–15 μ m) (Grace Davison Discovery Sciences). The hydroxylated peptide was eluted using a gradient of acetonitrile in 0.1% trifluoroacetic acid and then lyophilized. To prepare the peptide for NMR analysis the sample was resuspended in 160 μ l of methanol- d_4 and transferred to a 3-mm NMR tube. All NMR experiments were performed at 298 K on a Bruker AVIII 700 spectrometer equipped with an inverse TCI cryoprobe optimized for 1H observation and running TOPSPIN 2 software. HSQC spectra were collected using adiabatic 180 $^{\circ}$ CHIRP pulses, and TOCSY experiments employed the DIPSI-2 isotropic mixing scheme with mixing times of 120 ms. Spectra are referenced to residual methanol solvent signals at δ_H 3.33 and δ_C 48.0 ppm.

Bioinformatic Analyses—The SMART, PFAM, and Uniprot databases were searched for human ankyrin sequences. Sequences that were represented incompletely in the electronic resources were extended to the canonical length of 33 residues. To eliminate redundancy, AR matching to different entries for identical proteins was removed. Among the 1505 human AR sequences identified, 1354 ARs have a length of 32, 33, or 34 residues and were selected for the alignment.

Crystallography—The FIH Q239H variant was prepared by standard methodology and purified as described for wt FIH (3). Co-crystallization of FIH Q239H with the Asp-substrate peptide 2, HLEVVKLLLEHGADVDAQDK (purchased from PeptideSynthetics), used conditions reported for the FIH-HIF1 α CAD complex (25). A dataset for an FIH Q239H·Zn(II) NOG·Peptide 2 crystal was collected at the Diamond beamline I02 with an ADSC Q315 3 \times 3 CCD detector and was processed with HKL2000 (24). The structure was solved by molecular replacement using PHASER (search model PDB ID 1H2K) and was initially refined with CNS (25). Iterative cycles of model building in COOT (26) and slow cool-simulated annealing refinement using the maximum-likelihood function and bulk-solvent modeling in CNS proceeded until the decreasing R/R_{free} no longer converged. PROCHECK (27) was used to monitor the geometric quality of the model between refinement cycles and identify poorly modeled areas needing

Repeat	Sequence	Residue Number
Consensus	-G-TPLHPAA--GH--ΨV-ΨLL--GA--N----	
Repeat 1	DAATSFLRAARS ^{GNL} DKALDHLRNGVDI ^{N} TCNQ	43 (N39)
Repeat 2	NGLNGLHLASKEGHV ^{KMV} V ^{ELL} HKEIILETTTK	76
Repeat 3	KGNTALHIAALAGQDEVVREL ^{VNY} GANV ^{NA} QSQ *	109 (N105)
Repeat 4	KGFTPLYMAAQENHLE ^{VVK} F ^{LLE} NGAN ^{Q} NVATE *	142 (N138)
Repeat 5	DGFTPLAVALQQGHENVVAHLL ^{NY} GTGK K	171
Repeat 6	VRLPALHIAARNDDTRTAAVLLQNDPNPDVLSK	204
Repeat 7	TGFTPLHIAAHYENLNVAQLLLNRGSSV ^{N} FTPO *	237 (N233)
Repeat 8	NGITPLHIASRRGNV ^{IM} V ^{RL} LLDRGAQIETKTK	270
Repeat 9	DELTPLHCAARNGHVRISEILLDHGAPIQATTK	303
Repeat 10	NGLSPIHMAAQGDHLD ^{CV} RLLLQYDAEIDDITL	336
Repeat 11	DHLTPLHVAAHCGHHRVAKVLLDKGAKP ^{N} SRAL	369 (N365)
Repeat 12	NGFTPLHIACKKNHVRV ^{MEL} L ^{LKT} GTASIDAVTE	402
Repeat 13	SGLTPLHVAASFMGHLPIVKNLLQ ^{R} GASPNVSNV	435 (N431)
Repeat 14	KVETPLHMAARAGHTE ^{V} AKYLLQ ^{N} AKAK ^{N} AKAK *	468 (N464)
Repeat 15	DDQTPHCAARIGHTNMV ^{K} LLLENNANPN ^{L} LATT	501 (N497)
Repeat 16	AGHTPLHIAAREGHVETV ^{L} ALLEKEASQACMTK	534
Repeat 17	KGFTPLHVAAYGKVRVAE ^{L} LLERDAHP ^{N} AAGK	567 (N563)
Repeat 18	NGLTPLHVAVHNNL ^{D} IVKLLPRGGSPHSPAW	600
Repeat 19	NGYTPLHIAARQ ^{N} QVEVARSL ^{L} QYGGGSAN ^{A} ESV *	633 (N629)
Repeat 20	QGVTPHLHAAQEGHAEMV ^{ALL} SKQANG ^{N} LGNK	666 (N662)
Repeat 21	SGLTPLHLVAQEGHVPV ^{D} VLLKHGVMVDATTR	699
Repeat 22	MGYTPLHVASHYGNIK ^{L} VK ^{F} LLQHQADV ^{N} AKTK *	732 (N728)
Repeat 23	LGYSPLHQAAQQGHT ^{D} IVT ^{L} LLKNGASPN ^{E} VSS	765 (N761)
Repeat 24	DGTTPLAIAKRLGYISVTDV ^{L} KVVTDETSFV ^{L} V	798

FIGURE 1. Sequence alignment of the human ankyrinR ARD. The sequences of the 24 ARs of human ankyrinR were aligned to the consensus sequence by Michaely *et al.* (29). Ψ indicates a non-polar residue. Repeat numbers are on the left, and amino acid residue numbers on the right. Asn residues at positions analogous to demonstrated sites of FIH-catalyzed hydroxylation are highlighted in bold, and their residue numbers are given in parenthesis. The sequences of the synthesized peptides are underlined. Asterisks indicate peptides observed to be FIH substrates (see supplemental Fig. S1).

attention. The final model was refined with a round of REFMAC TLS using the anisotropic thermal motion parameters derived from TLS motion determination server (28). 90.4% of the residues in the final model lie within the most favored regions of the Ramachandran [φ, ψ] plot and the rest within the additionally allowed regions. For data collection and refinement statistics, see supplemental Table S1. The coordinates for the structure have been deposited in the Protein Data Bank under accession code 2xum.

RESULTS

FIH Hydroxylates Peptide Fragments Derived from Cytoskeletal Ankyrins—Sequence analyses of the 24 ARs of human ankyrinR identified 13 Asn residues at positions analogous to previously demonstrated sites of FIH-dependent hydroxylations (5–9) (Fig. 1). To investigate which of these ARs contain Asn residues that are FIH substrates, we synthesized peptides spanning the potential hydroxylation sites and tested them in FIH incubation assays. Peptides corresponding to ARs 3, 4, 7, 14, 19, and 22 of the ankyrinR ARD displayed an increase of 16 Da in mass to varying extents after incubation with FIH (Fig. 1 and supplemental Fig. S1). MS/MS analyses of the modified peptides assigned the sites of hydroxylation to Asn residues corresponding to Asn-105, Asn-233, Asn-464, Asn-629, and Asn-728 in ankyrinR ARD (supplemental Figs. S2–S6). We next examined the sequences of the other human cytoskeletal proteins, ankyrinB and ankyrinG, and found several Asn residues located at analogous hydroxylation positions to ankyrinR (supplemental Figs. S7A and S8A). Synthetic peptides spanning ankyrinB Asn-58, Asn-124, Asn-656, and

Asn-755 and ankyrinG Asn-68, Asn-134, Asn-658, Asn-691, and Asn-757 were all found to be hydroxylated by FIH (supplemental Figs. S7B and S8B). The observations suggested that the human cytoskeletal ankyrins are potential FIH substrates.

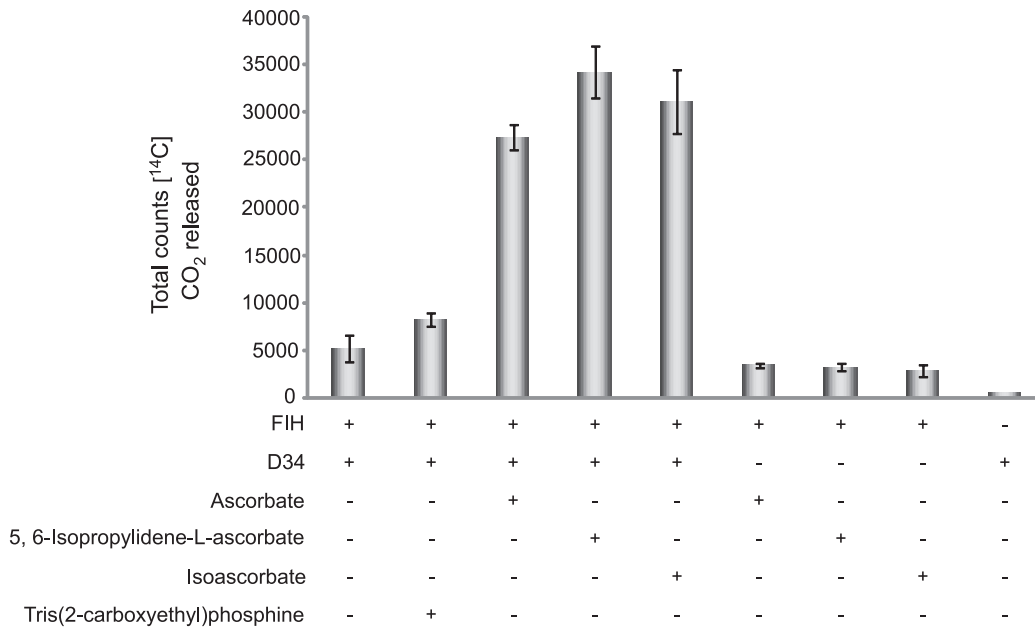
Ankyrin ARDs Are Multiply Hydroxylated by FIH—To assess whether the residues hydroxylated in the peptide studies above could also be hydroxylated in the context of an ARD, we first purified recombinant human ARDs from *Escherichia coli*. We were successful in isolating the C-terminal 12 ARs of ankyrinR (residues 402–827; D34) (29) and the 24 ARs of ankyrinB (residues 1–959) (30) in sufficient quantity and purity for further analyses. Initially, we tested whether ankyrinR D34 stimulates FIH activity using a 2OG decarboxylation assay (3). Because the activities of some 2OG oxygenases are stimulated by reducing agents including ascorbate (31–33), we also tested the effect of ascorbate and its analogues on D34 turnover by FIH. D34 promoted higher levels of 2OG decarboxylation in the presence of ascorbate, IPAA, or D-isoascorbate than in their absence (Fig. 2A). Hydroxylated D34 material was produced by bacterial co-expression of vectors encoding for GST-tagged D34 and His-tagged FIH, with the supplementation of exogenous Fe(II), 2OG, and IPAA to the bacterial cell culture. LC/MS and MS/MS analyses of the purified D34 assigned sites of hydroxylation to residues Asn-431 (50%), Asn-464 (95%), Asn-629 (88%), Asn-662 (8%), Asn-728 (69%), and Asn-761 (23%) (Fig. 2B, supplemental Figs. S9–S14). Interestingly, the Asn-431, Asn-662, and Asn-761 sites were not found to be hydroxylated in the studies employing 18-residue synthetic peptides (Table 1 and data not shown), suggesting “catalytically productive” folding within the ARD promotes hydroxylation at these sites. In addition to the Asn hydroxylations, an unprecedented FIH-catalyzed aspartate hydroxylation was identified at Asp-695 (15%) in D34 purified from bacteria co-expressing FIH (supplemental Fig. S15).

To test whether ankyrinB protein is also an FIH substrate, we incubated recombinant ankyrinB ARD with FIH under our standard assay conditions. Consistent with the peptide studies, trypsinolysis and MS analyses of the reacted ankyrinB observed hydroxylation in the tryptic peptides containing Asn-58 (68%), Asn-124 (74%), and Asn-656 (71%) (supplemental Fig. S16). Interestingly, hydroxylation of an aspartate residue (Asp-491) was also identified (15%, supplemental Fig. S17), suggesting that the ankyrinB ARD is also a substrate for FIH-catalyzed Asn and Asp hydroxylation.

D34 Is a Substrate for FIH in HEK293T Cells—To test if a cytoskeletal ARD is an FIH substrate in animal cells, we immunopurified V5-tagged D34 from HEK293T cells expressing endogenous levels of FIH. Under these conditions the expression level of D34 was significantly higher than that of FIH; as a result, we identified only ~3% Asn hydroxylation at Asn-728 in D34 (the peptide fragment containing Asn-464 was not detected; only unhydroxylated forms were detected for the fragments containing Asn-431, Asn-629, Asn-662, and Asn-761; data not shown). However, MS analyses of D34 purified from HEK293T cells overexpressing wild type FIH, but not the hydroxylase defective FIH D201A variant (34), led to detection of Asn hydroxylations at Asn-431 (54%), Asn-629

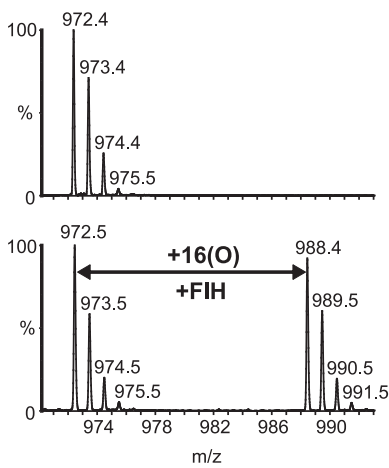
Ankyrin Asparagine and Aspartate Hydroxylation by FIH

A



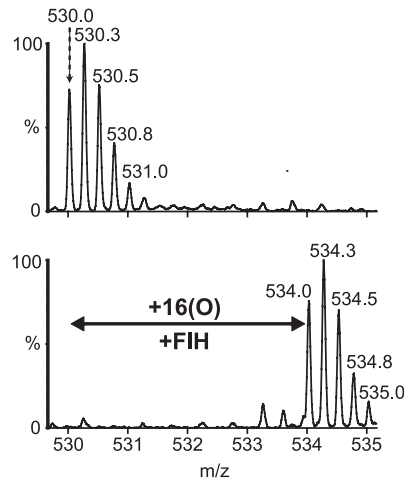
B1

GASPNVSNVK (N431)



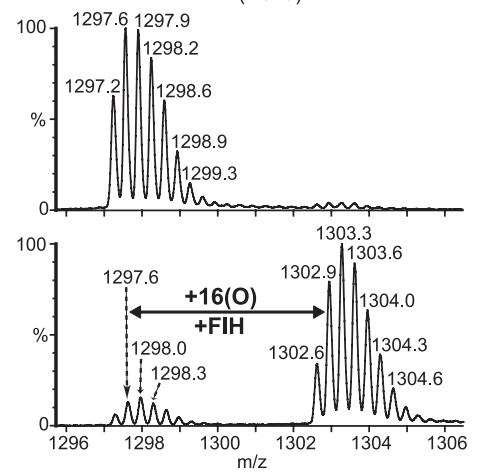
B2

VAKYLLQNKAKVNAKAKDD (N464)



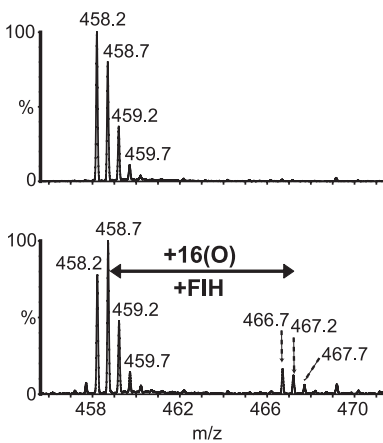
B3

SLLQYGGSANAESVQGVTPHLHAAQEGHAEMVALLSK (N629)



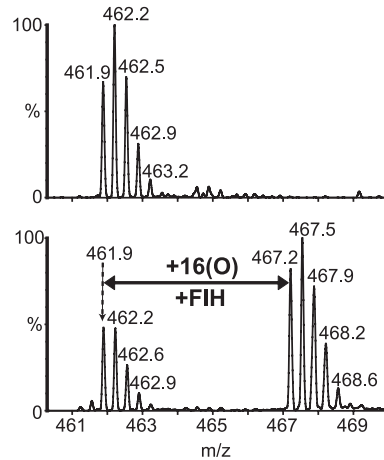
B4

QANGNLGNK (N662)



B5

FLLQHQADVNAK (N728)



B6

NGASPNEVSSDGTPLAIK (N761)

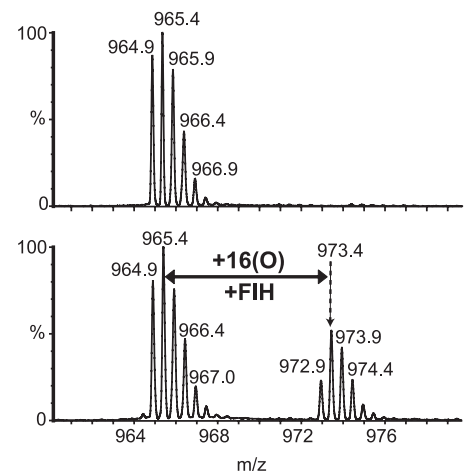


TABLE 1

Summary of the Asn and Asp hydroxylation sites within the ankyrinR ARD identified by MS analyses of synthetic ankyrinR peptides, of recombinant D34 co-expressed with FIH in *E. coli* or HEK293T cells, and of full-length endogenous ankyrinR purified from human or mouse erythrocytes

AR	sequence	OH site	Hydroxylations detected from				
			18mer peptide	D34 from <i>E. coli</i>	D34 from 293T	AnkyrinR from human**	AnkyrinR from mouse
1	DAATSFLRARRSGNLDKALDPRNGVDLTCNQ		×			-	-
2	NGLNGDHSKKEGHVHMVDEHKEIILETTTK		×			×	×
3	KKPKLHIALAGQDEVVREINYGANVWQSQ	N105	✓			26%, 34%	15%, 17%
4	KKPKLHIAQENHLEVVKLENGANGQATE	N138	✓*			20%, 27%	14%*
5	TKPKLHIAVLLQGHENVVAFINNYGTGK K		×			-	-
6	VRLLPDLHIAARRNDTRTAAYDNDPNDFVLSK		×			×	×
7	TKPKLHIAHYENLNVAQLDNRGSSNTEFQ	N233	✓			35%, 54%	×
8	NSPKLHIAARRGNVIMVRLDRGAQIETKTK		×			-	-
9	DELPKLIHIAARRNGHVRVISEIDHGAPIQAKTK		×			×	×
10	NSLSEHIAAAGDHLDCVRLDYDAEIDDTL		×			-	-
11	DHLPKLIHIAARRGHHRVAKVLEKGAKEISRAL		×			-	-
12	NSPKLHIAARRKKNHVRVMELEKKGASIDAVTE		×			×	-
13	SEPKLHIAARRFMGHLPIVKKLDRGASVNSV	N431	×	50%	54%	×	×
14	KVEPKLHIAARRAGHTEVAKVLEKNGAKVNAKAK	N464	✓	95%	-	-	-
15	DDGPKLHIAARRIGHNTNPKLENNANENHATT	N497	×	7%*	19%*	×	×
16	AKPKLHIAARRRGHVEVTLADLKEKASQACMTK		-	-	-	-	-
17	KSPKLIHIAARRKYGKVRVAELERDRAHENVAGK		×	×	×	×	×
18	NSPKLHIAARRVHNNLDIVKLEPRGGSHPHAW		×	×	×	×	×
19	NSPKLHIAARRKQVQVARELEQVGSNNEVESV	N629	✓	88%	94%	×	×
20	CKPKLHIAARRQGHAEVVALDRSQANGNKNK	N662	×	8%	-	×	-
21	SEPKLHIAARRGHPVVDVLEKHGVMVDATTR	N695	×	15%	16%	×	×
22	MSPKLHIAARRSHYGNIRLVKLEHQADVNAKTK	N728	✓	69%	95%	6%, 21%*	-
23	ISYSKLIHIAARRAQQGHTDIVTLEKNGASENEVSS	N761	×	23%	30%	×	×
24	KPKLHIAARRKRLGYISVTDVLEKVVTDTSFVLV	F795	-	×	11%	×	×

✓ Hydroxylation was unequivocally assigned by LC/MS and MS/MS analyses.

× The corresponding unhydroxylated tryptic or endoproteinase Glu-C peptide was detected, but no +16-Da species was observed.

- The corresponding unhydroxylated peptide was not detected.

* A +16-Da mass shift was observed, but the hydroxylated residue was not covered by MS/MS analyses.

** Two independent blood samples from the same laboratory donor were used to isolate endogenous ankyrinR, and the ratios are shown for each preparation. MS analysis of the same sample was performed twice, and the variation observed between the two biological replicates was greater than the analytical repeats.

(94%), Asn-728 (95%), and Asn-761 (30%) as well as Asp hydroxylation at Asp-695 (16%) (supplemental Figs. S18–S23). Oxidation of a phenylalanine residue (Phe-795) of D34 was also identified (11%) (supplemental Fig. S24). Although its biological relevance is unclear, the fact that this modification was not modulated by FIH overexpression (supplemental Fig. S24) and was not present in D34 purified from *E. coli* (data not shown) suggests that other mammalian oxygenases may target ankyrinR.

Endogenous AnkyrinR Is Hydroxylated—We next investigated the hydroxylation status of endogenous ankyrinR. AnkyrinR was purified from human erythrocytes essentially as described by Bennett and Stenbuck (22) and resolved by SDS-PAGE analysis (Fig. 3A). MS analyses of the in-gel tryptic digests identified ankyrinR (Swiss-Prot accession number P16157) with a Mascot score of 8864 and a sequence coverage

of 57% (132 peptides assigned). Consistent with the *in vitro* peptide studies (Table 1), Asn-105 (26–34%), Asn-138 (20–27%), and Asn-233 (35–54%) in endogenous ankyrinR were sufficiently hydroxylated to be assigned by MS/MS analyses (Fig. 3, B and C, and supplemental Figs. S25–S27). Consistent with the analyses of *E. coli* purified D34, Asn-728 was also likely hydroxylated (6–21%) in endogenous ankyrinR because a +16-Da mass peak eluted just before the unhydroxylated tryptic peptide (supplemental Fig. S25C and data not shown). These elution characteristics are consistent with Asn hydroxylation as described previously (5, 6, 8), although MS/MS data for the hydroxylated fragment containing Asn-728 were not obtained due to insufficient signal intensity. Asn hydroxylation of other sites detected in material purified from HEK293T cells or *E. coli* was not detected (Table 1). To investigate whether ankyrinR ARD hydroxylation is a conserved phenomenon in animals, we purified mouse endogenous ankyrinR (Swiss-Prot accession number Q02357, Mascot score 3711, sequence coverage 43%, 61 peptides assigned) as for the human protein. Although the reduced purification scale hampered analyses, hydroxylation of 1 Asn residue, Asn-105 (15–17%), was also identified in mouse ankyrinR (supplemental Fig. S28). Interestingly, sequence alignment of mammalian ankyrinR ARDs indicates that the other hydroxylation sites identified in this study are also well conserved (supplemental Fig. S29).

In addition to Asn hydroxylations, an oxidation was detected at Trp-1454 within the regulatory domain of ankyrinR isolated from the human. MS analyses revealed both +16- and +32-Da mass shifts at this tryptophan residue (supplemental Fig. S30). Although the regioselectivity of the apparent tryptophan oxidation was not assigned from the MS data, this observation is consistent with previous reports of oxidation of tryptophan to hydroxytryptophan and *N*-formylkynurenine residues (35–40). The biological significance of the observed Trp-1454 oxidation is unknown.

Hydroxylation Increases the Conformational Stability of D34—Previously we showed that Asn hydroxylation increases the conformational stability of the ankyrin-fold of an artificial consensus ARD (17, 18). To determine whether FIH-catalyzed hydroxylation increases the conformational stability of a natural and structurally important ARD, we investigated the effect of hydroxylation on the stability of D34 using circular dichroism (CD) and DSC. CD monitored thermal denaturation followed by ellipticity changes at 222 nm revealed sigmoidal unfolding curves with a single sharp transition for both D34 and D34-OH (Fig. 4A). The thermal denaturation was irreversible,

FIGURE 2. **Recombinant D34 is hydroxylated by FIH.** A, D34 promotes FIH-dependent 2OG decarboxylation in the presence of ascorbate or its analogues. Assays were carried out in triplicate. B1–B6, LC/MS spectra of trypsin or endoproteinase Glu-C digested fragments derived from D34 purified from *E. coli* or D34 purified from *E. coli* cells co-expressing FIH are shown. B1, LC/MS spectra showing the non-hydroxylated ($[M+H]^+ = m/z$ 972.5) and hydroxylated ($[M+H]^+ = m/z$ 988.5) forms of the 427–436 (GASPNVSNVK) tryptic peptide containing Asn-431 are shown. B2, LC/MS spectra showing the non-hydroxylated ($[M+4H]^{4+} = m/z$ 530.0) and hydroxylated ($[M+4H]^{4+} = m/z$ 534.0) forms of the 452–469 (VAKYLLQNKAKVNAKAKDD) endoproteinase Glu-C peptide containing Asn-464 are shown. B3, LC/MS spectra showing the non-hydroxylated ($[M+3H]^{3+} = m/z$ 1297.2) and hydroxylated ($[M+3H]^{3+} = m/z$ 1302.6) forms of the 620–657 (SLLQYGGSAANAESVQGVTPHLAAQEGHAEMVALLLSK) tryptic peptide containing Asn-629 are shown. B4, LC/MS spectra showing the non-hydroxylated ($[M+2H]^{2+} = m/z$ 458.2) and hydroxylated ($[M+2H]^{2+} = m/z$ 466.2) forms of the 658–666 (QANGNLGNK) tryptic peptide containing Asn-662 are shown. B5, LC/MS spectra showing the non-hydroxylated ($[M+3H]^{3+} = m/z$ 461.9) and hydroxylated ($[M+3H]^{3+} = m/z$ 467.2) forms of the 719–730 (FLLQHQADVNAK) tryptic peptide containing Asn-728 are shown. B6, LC/MS spectra showing the non-hydroxylated ($[M+2H]^{2+} = m/z$ 964.9) and hydroxylated ($[M+2H]^{2+} = m/z$ 972.9) forms of the 756–775 (NGASPNEVSSDGTTPLAIAK) tryptic peptide containing Asn-761 are shown. See supplemental Figs. S9–S14 for MS/MS assignments of hydroxylation to residues Asn-431, Asn-464, Asn-629, Asn-662, Asn-728, and Asn-761, respectively.

Ankyrin Asparagine and Aspartate Hydroxylation by FIH

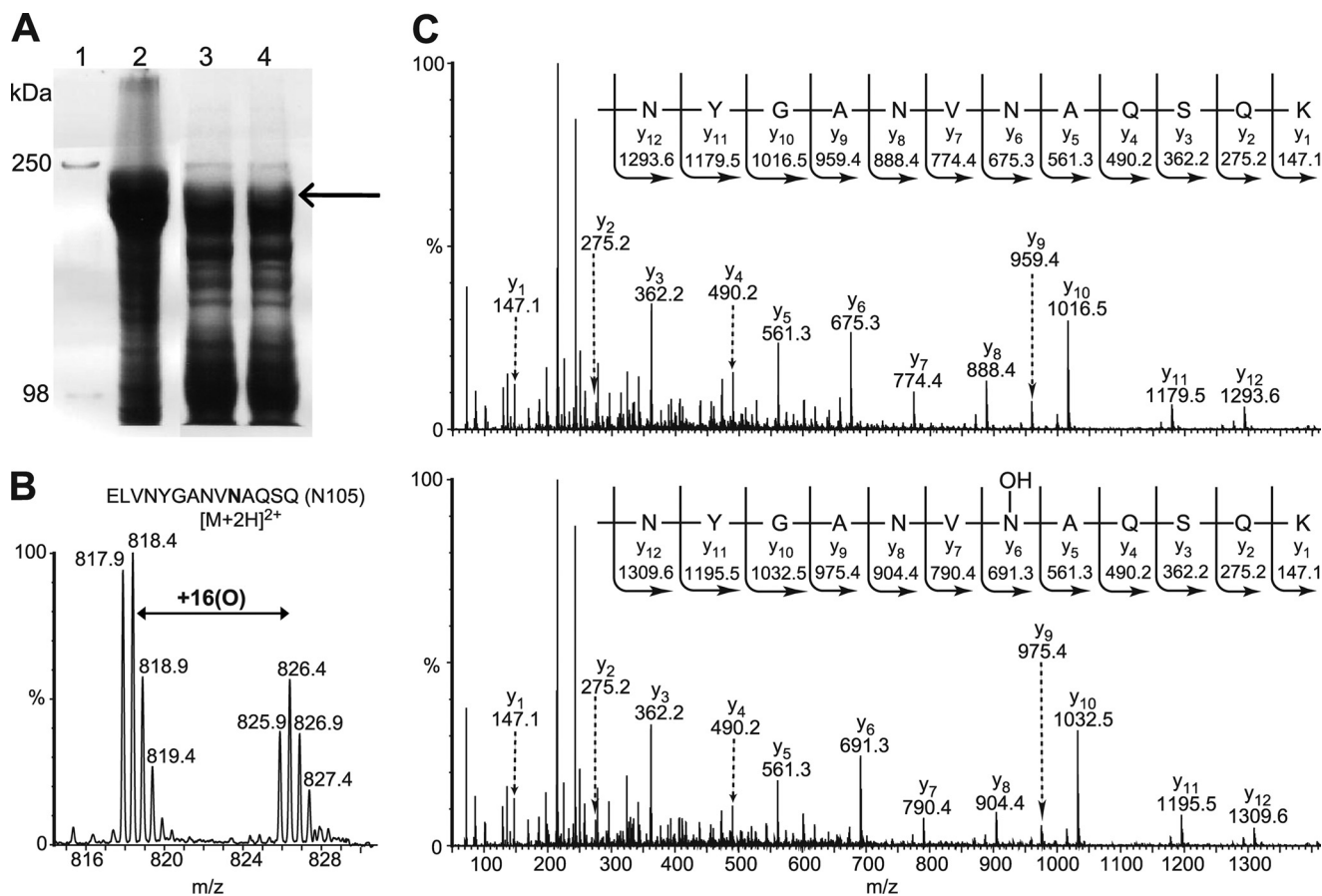


FIGURE 3. Human erythrocyte ankyrinR is hydroxylated. A, SDS-PAGE analysis shows the purification of endogenous ankyrinR from a human. Isolated erythrocyte ghosts were washed using Triton X-100, the remaining pellet was extracted using 2 M KCl, and the supernatant from the KCl extraction was dialyzed to remove the salt. Lane 1, M_r marker; lane 2, erythrocyte ghost; lanes 3 and 4, dialyzed supernatant from the KCl extraction. The arrow indicates where ankyrinR was identified by tryptic digestion and MS analyses. B, the LC/MS spectrum shows the unhydroxylated $[M+2H]^{2+} = m/z$ 817.9 and hydroxylated $[M+2H]^{2+} = m/z$ 825.9 forms of the 96–110 tryptic peptide containing Asn-105. C, MS/MS assignment of hydroxylation at Asn-105 in the 96–110 tryptic peptide in human endogenous ankyrinR is shown. A +16-Da mass shift is observed in the y ion series appearing at y_6 , corresponding to fragments containing Asn-105.

precluding a deeper thermodynamic analysis of the data. Therefore, we report only the apparent T_m values here. The T_m value for D34 was 52.2 °C, whereas a value of 55.3 °C was observed for D34-OH, suggesting that the hydroxylated protein is thermally more stable. In keeping with this proposal, thermal denaturation analyses monitored by DSC revealed a clear stabilizing effect for D34-OH compared with D34 ($T_m = 50.3$ °C for D34 and 53.6 °C for D34-OH) (Fig. 4B).

The urea-induced equilibrium unfolding of D34 monitored by CD analyses revealed the presence of a possible intermediate state as indicated by a shoulder in the sigmoidal denaturation curves (Fig. 4C). The denaturation data were fitted to a three-state model as described by Werbeck and Itzhaki (23). D34-OH displayed a similar unfolding pattern to D34; however, it was shifted to higher urea concentrations, characterized by an increase of ~ 0.4 M in the midpoint of unfolding for both the native to the intermediate state (N \rightarrow I) and the intermediate to the unfolded state (I \rightarrow U) transitions (Fig. 4C), indicating that D34-OH is more resistant to urea-induced denaturation than D34. Taken together, these data suggest that FIH-catalyzed hydroxylations increase the stability of the D34-fold.

Hydroxylation Reduces the Affinity of D34 with CDB3—To investigate whether the increased conformational stability conferred by hydroxylation could modulate a known protein-protein interaction of ankyrinR, we studied its interaction with band 3. The ankyrinR ARD interacts with the cytoplasmic domain of band 3 (CDB3), thereby linking the erythrocyte membrane bilayer to the spectrin-based cytoskeleton, which in turn regulates the mechanical and morphological properties of the erythrocyte membrane (41, 42). The D34 region of the AnkyrinR ARD contains a high affinity binding site for band 3 and recapitulates the binding properties of the full ARD (43), whereas the D2 region (ARs 7–12) also contains a band 3 binding site of lower affinity (41). To test for an effect of D34 hydroxylation on its interaction with CDB3, we co-expressed V5-tagged D34 and FLAG-tagged CDB3 (aa 2–379) in HEK293T cells in the presence and absence of overexpressed FIH. Immunoprecipitation of V5-tagged D34 followed by immunoblotting for the presence of associated FLAG-CDB3 showed that the extent of interaction between D34 and CDB3 was significantly reduced upon overexpression of wild type FIH but not the hydroxylase-defective FIH D201A mutant (Fig. 4D), consistent with a

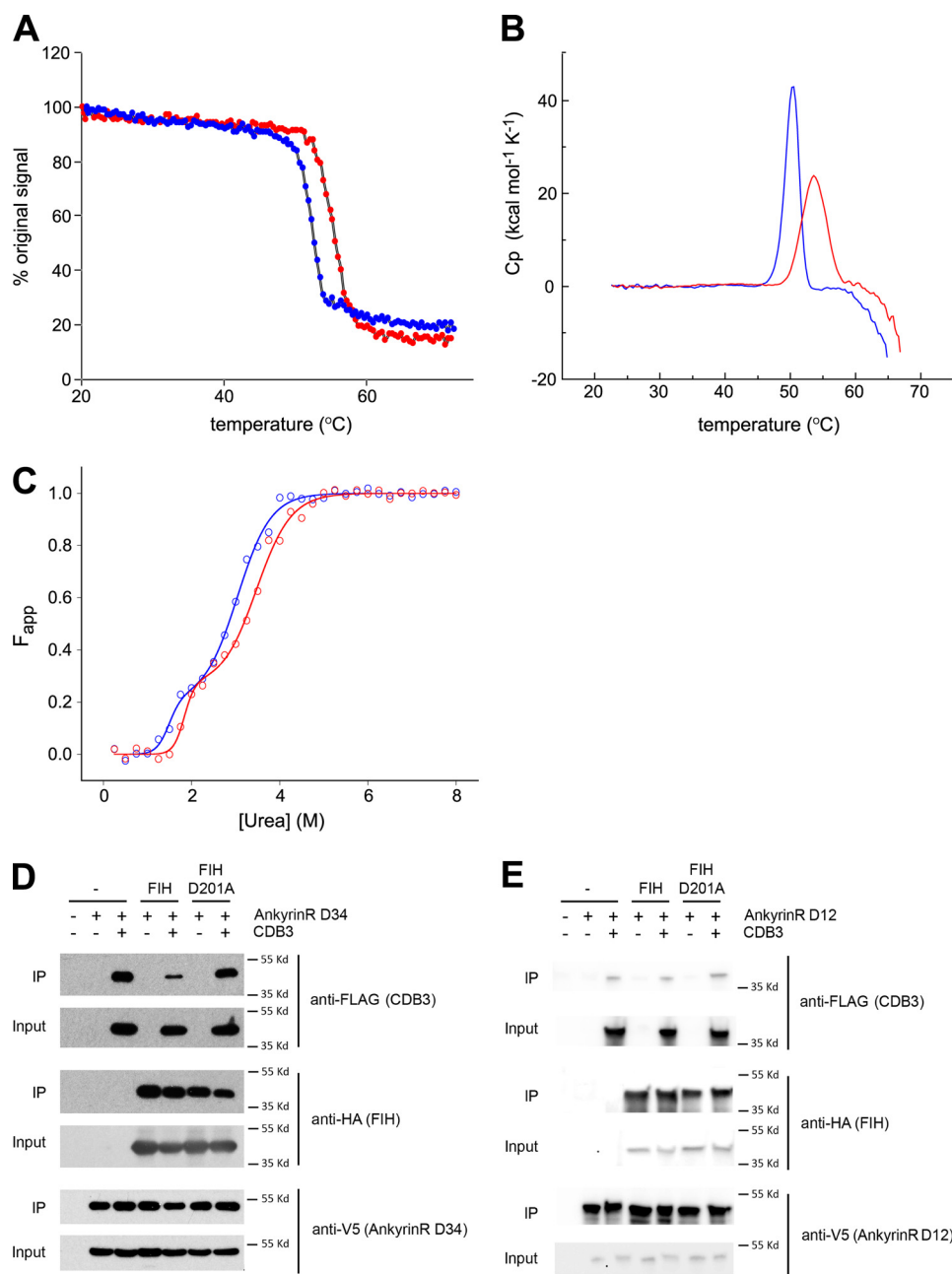


FIGURE 4. Biophysical effects of D34 hydroxylation. A–C, hydroxylation increases the conformational stability of D34. Data are representative of two independent experiments. A, temperature-induced denaturation of D34 (blue) and D34-OH (red) monitored by CD spectroscopy at 222 nm is represented as the percentage of the original signal at 20 °C. The midpoint of the unfolding transitions (T_m) was 52.2 °C for D34 and 55.3 °C for D34-OH. B, DSC monitored temperature induced denaturation data for D34 and D34-OH after base-line correction and normalization is shown. The melt temperatures obtained were 50.3 °C for D34 and 53.6 °C for D34-OH. C, shown is urea-induced equilibrium unfolding of D34 and D34-OH (open circles) fitted to a three-state model (23) (solid line) using SigmaPlot. The midpoints of unfolding (D_{50}) was obtained from the curve fit as follows: $D_{50\text{N} \rightarrow \text{I}} = 1.5$ M for D34 and 1.8 M for D34-OH; $D_{50\text{I} \rightarrow \text{U}} = 3.0$ M for D34, and 3.5 M for D34-OH. D, hydroxylation reduces the interaction of D34 with CDB3. Immunoblot analyses of the interaction of D34 with CDB3 in the presence or absence of FIH overexpression is shown. V5-tagged D34 was immunoprecipitated from HEK293T cells co-expressing FLAG-CDB3 (aa 2–379) in the presence or absence of wild type or D201A HA-tagged FIH. The resultant complexes were immunoblotted for CDB3, D34, and FIH. IP, immunoprecipitate. E, hydroxylation does not alter the interaction between D12 and CDB3. Immunoblot analyses of the interaction of D12 with CDB3 in the presence or absence of FIH overexpression are shown. V5-tagged D12 was immunoprecipitated from HEK293T cells co-expressing FLAG-CDB3 (aa 2–379) in the presence or absence of wild type or D201A HA-tagged FIH. The resultant complexes were immunoblotted for CDB3, D12, and FIH. Cp, specific heat capacity at constant pressure; F_{app} , apparent fraction of unfolded protein.

role for FIH-dependent hydroxylation in modulating the ankyrinR/CDB3 interaction. In contrast, overexpression of FIH did not modulate the affinity of CDB3 for D12 (aa 1–402, ARs 1–12), which encompasses the D2 region that is a second ankyrinR-CDB3 interaction site (41) (Fig. 4E). To investigate whether the effect of FIH on binding of D34

to CDB3 was direct, we performed pulldown assays using GST-tagged non-hydroxylated (GST-D34) and hydroxylated D34 (GST-D34-OH) to capture His-tagged recombinant CDB3 *in vitro*. Consistent with a direct role for FIH-mediated hydroxylation in reducing the affinity of ankyrinR for CDB3, significantly less CDB3 was pulled

Ankyrin Asparagine and Aspartate Hydroxylation by FIH

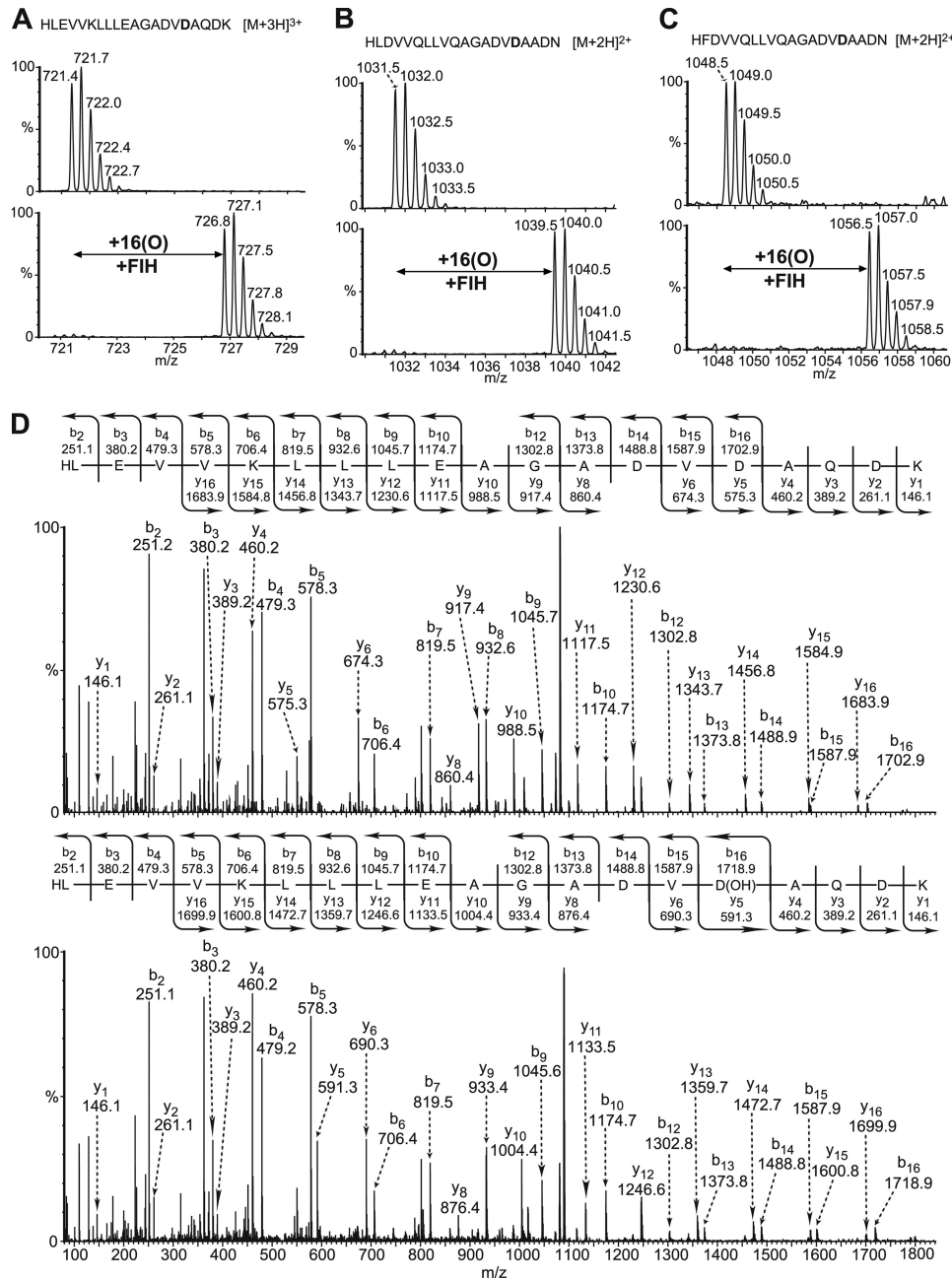


FIGURE 5. FIH is an aspartate hydroxylase. 20-Residue synthetic peptides derived from naturally occurring or consensus AR sequences were incubated in the absence or presence of FIH under standard assay conditions. The desalted incubation products were subjected to LC/MS and MS/MS analyses. **A**, LC/MS spectra of the non-hydroxylated ($[M+3H]^{3+} = m/z$ 721.4) and hydroxylated ($[M+3H]^{3+} = m/z$ 726.8) forms of the consensus ankyrin peptide HLEVVKLLLEAGADVDAQDK are shown. **B**, LC/MS spectra of the non-hydroxylated ($[M+2H]^{2+} = m/z$ 1031.5) and hydroxylated ($[M+2H]^{2+} = m/z$ 1039.5) forms of a synthetic peptide derived from the human ARD protein GTAR (Swiss-Prot accession number O75179, aa 1365–1384, HLDVVQLLVQAGADVDAADN). **C**, LC/MS spectra of the non-hydroxylated ($[M+2H]^{2+} = m/z$ 1048.5) and hydroxylated ($[M+2H]^{2+} = m/z$ 1056.5) forms of a synthetic peptide derived from the human ARD protein MASK (Swiss-Prot Accession Q81WZ3, aa 1337–1356, HFDVVQLLVQAGADVDAADN) are shown. **D**, MS/MS assignment of hydroxylation to the Asp residue at the conserved hydroxylation position in the consensus AR peptide shown in **A** is shown.

down by GST-D34-OH than GST-D34 (supplemental Fig. S31).

FIH-catalyzed Asp Hydroxylation of ARDs May Be a Common Modification—Bioinformatic analyses of 1505 human AR sequences obtained from the SMART and PFAM databases revealed that, after asparagine, aspartate is the second most commonly occurring residue at the conserved FIH-catalyzed hydroxylation position, with 475 occurrences for asparagine and 240 for aspartate (supplemental Fig. S32). To inves-

tigate the possibility that FIH catalyzes the Asp hydroxylation of other ARs, we placed an Asp residue in an ankyrin peptide with a consensus sequence (Peptide 1, HLEVVKLLLEAGADVDAQDK) (17, 44) and tested it as an FIH substrate. A +16-Da mass increase was indeed observed after incubation of Peptide 1 with FIH under standard assay conditions, and MS/MS analyses of the modified peptide assigned hydroxylation to the target Asp residue (Fig. 5, **A** and **D**). To compare the efficiency of the FIH-catalyzed Asp versus Asn hydroxyla-

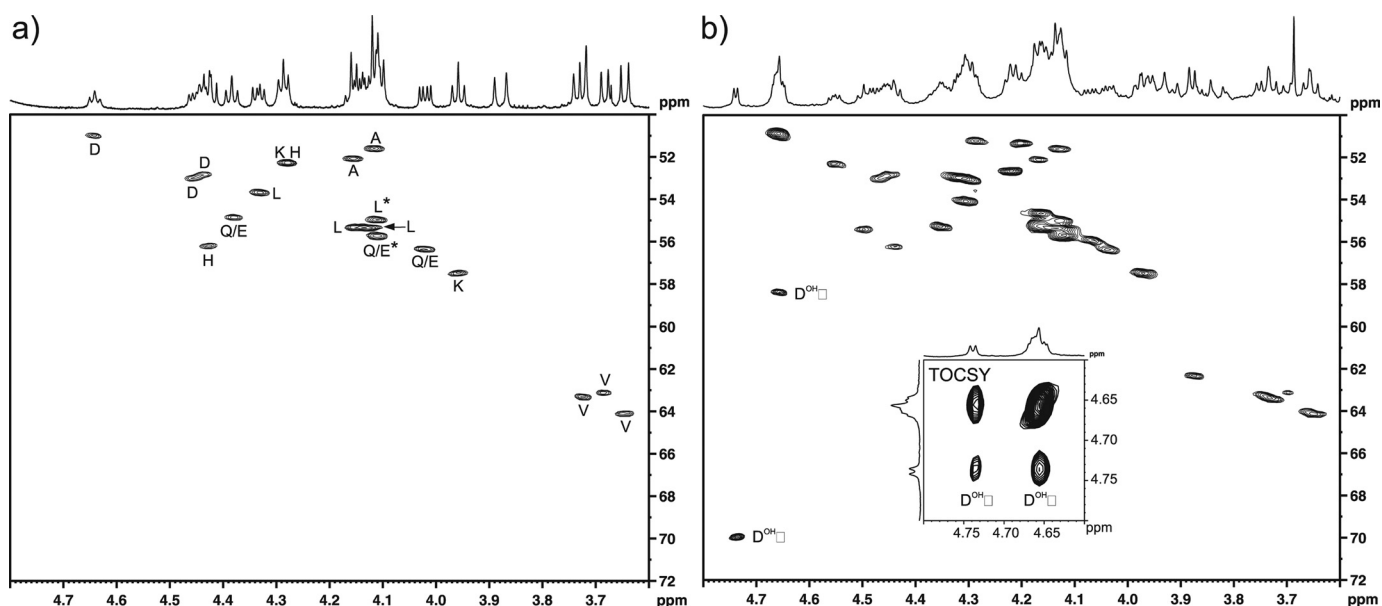


FIGURE 6. FIH-catalyzed Asp hydroxylation occurs at the β -position. Hydroxylated Peptide 2 (HLEVVKLLEHGADVDAQDK) was produced by incubation with FIH under standard assay conditions (hydroxylated to $\sim 75\%$ as assessed by MALDI-TOF analyses), purified by reverse phase HPLC, and analyzed by NMR spectroscopy. *a*, shown is the α -proton region of the $^{13}\text{C}, ^1\text{H}$ one-bond correlation spectrum (HSQC) of the Asp-substrate Peptide 2 in methanol- d_4 with amino acid assignments indicated (Gly residue not included; Gln and Glu resonances have not been differentiated; *, assignments may be interchanged owing to ^1H overlap). *b*, shown is the $^{13}\text{C}, ^1\text{H}$ one-bond correlation spectrum (HSQC) of the HPLC-purified incubation product (both unhydroxylated and the hydroxylated peptide are present). Resonances arising from the α - and β -hydrogens of the hydroxylated Asp residue are indicated, and the $^1\text{H}, ^1\text{H}$ correlation arising from the three-bond coupling between these is apparent in the TOCSY spectrum (*inset*).

tions, we tested consensus ankyrin peptides containing either an Asn or an Asp residue at the conserved hydroxylation position under the same assay conditions. Both the 20-residue DVNA and DVDA motif-containing AR peptides were $>90\%$ hydroxylated under the assay conditions used; however, when the N-terminal two residues were truncated, the 18-residue DVDA AR peptide was hydroxylated to only $\sim 12\%$, whereas the 18-residue DVNA AR peptide was $>90\%$ hydroxylated (supplemental Fig. S33). These results suggest that within the same sequence background, the FIH-dependent hydroxylation of the Asn residue is more efficient than that of Asp residue. Consistent with this proposal we found that the FIH D201G variant, which retains Asn hydroxylation activity, did not catalyze ($<5\%$) the hydroxylation of an Asp-containing peptide with the same sequence frame under standard incubation conditions (supplemental Fig. S34). To investigate if FIH also hydroxylates Asp residues in other naturally occurring ARs besides ankyrinR, we screened for synthetic peptides derived from naturally occurring ankyrin repeat sequences as substrates for FIH-dependent Asp hydroxylation (supplemental Table S2). The peptide fragments derived from the ARD protein GTAR (Gene Trap Ankyrin Repeat, Swiss-Prot O75179, aa 1365–1384, HLDVVQLLVQAGADVDAADN) and the ARD protein hMASK (Multiple Ankyrin repeats Single KH domain, Swiss-Prot Q81WZ3, aa 1337–1356, HFDVVQLLVQAGADVDAADN) both displayed a +16-Da mass shift after reaction with FIH (Fig. 5, B and C). MS/MS analyses of the modified GTAR_{1365–1384} peptide assigned hydroxylation to the aspartate residue (Asp-1380) at the predicted hydroxylation position (supplemental Fig. S35). Although unequivocal MS/MS assignment for hydroxylation of hMASK_{1337–1356} was not obtained, the sequence of this peptide only differs by one

residue from the GTAR_{1365–1384} peptide; thus, hydroxylation is likely at an analogous position. These observations raise the possibility that FIH could potentially catalyze Asp hydroxylation in naturally occurring ARDs.

FIH-catalyzed Asp Hydroxylation Occurs on the β -Carbon—To investigate the regiochemistry of FIH-catalyzed Asp hydroxylation, we analyzed the hydroxylated and non-hydroxylated forms of an Asp-substrate peptide using NMR spectroscopy. In a separate line of work we found that replacing the alanine residue at the -5 position relative to the hydroxylation site of the consensus AR sequence with a histidine residue (17) increases the efficiency of FIH-catalyzed hydroxylations.⁵ Therefore, to optimize hydroxylation we synthesized the corresponding 20-residue AR peptide HLEVVKLLEHGADVDAQDK (Peptide 2) and assessed the ^1H and ^{13}C chemical shift changes between the unmodified peptide substrate and the HPLC-isolated incubation product by two-dimensional $^{13}\text{C}, ^1\text{H}$ HSQC and $^1\text{H}, ^1\text{H}$ TOCSY experiments (Fig. 6). In the HSQC spectrum of the modified Peptide 2 in d_4 -methanol (hydroxylated to $\sim 75\%$), two distinctive correlations were observed that could be ascribed to a β -hydroxylated aspartate residue and assigned to the α (δ_{H} 4.661, δ_{C} 58.39 ppm) and β (δ_{H} 4.741, δ_{C} 69.97 ppm) positions. A resolved ^1H doublet ($J = 4.7$ Hz) was observed for the β -proton that correlated to the hidden α -proton in the two-dimensional TOCSY experiment (Fig. 6b, inset), again consistent with the pattern expected for hydroxylation of the β -carbon. The ^{13}C chemical shifts in the hydroxylated aspartate correlate well with those observed previously for β -hydroxy aspara-

⁵ M. Yang, unpublished data.

Ankyrin Asparagine and Aspartate Hydroxylation by FIH

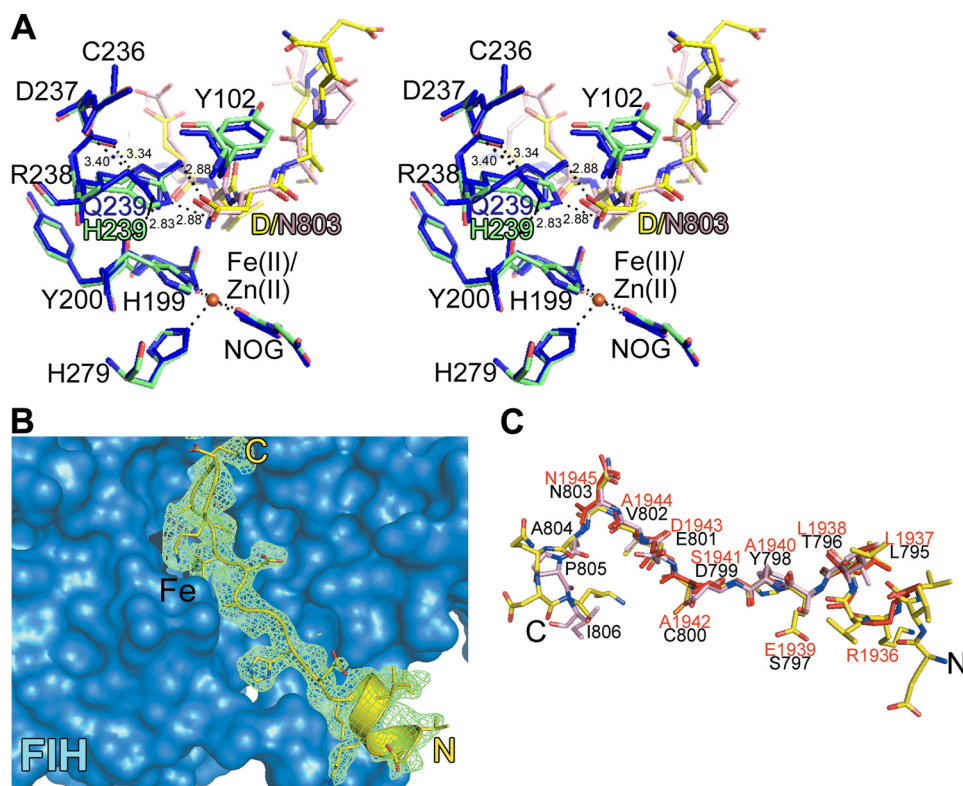


FIGURE 7. Binding of an Asp-substrate peptide at the FIH active site. A, shown is a stereoview derived from the crystal structures of the FIH Q239H+Peptide 2-Zn(II)-NOG and the FIH-HIF1αCAD (aa 786–826) Fe(II) NOG complexes. NOG is a 2OG analog, and Zn(II) substitutes for Fe(II). In the FIH Q239H+Peptide 2 complex structure, His-239 of variant FIH adapts a very similar position to that of Gln-239 in wt FIH such that the Ne2 of His-239 is positioned to hydrogen bond to Oδ2 of the substrate Asp residue in Peptide 2 (Ne2 His-239–Oδ2 Asp, 2.88 Å). A water molecule (not shown) with $\leq 50\%$ occupancy coordinates at the metal center (H_2O –Zn(II), 2.2 Å). The partial occupancy of this metal-coordinating water molecule may reflect the propensity of FIH to undergo a transition between 6- and 5-coordination states as observed for a structurally related dioxygenase (53). B, surface representation of the FIH Q239H+Peptide 2-Zn(II)-NOG complex at the N-terminal substrate binding site (Site 1) of FIH Q239H. Peptide 2 adopts a slightly different conformation compared with the HIF fragment (root mean square deviation for $\text{C}\alpha$ 0.62 Å, PDB ID 1H2K). C, shown is a stick representation of the superimposed Peptide 2 (yellow), HIF-1αCAD (*salmon*, residues 795–806), and notch1 (*red*, residues 1936–1945) substrates when bound to FIH.

gine (α , 56.26; β , 72.22 ppm in D_2O) (45) and for a reference sample of β -hydroxy aspartic acid (α , 57.86; β , 71.54 ppm in D_2O , pD 9).

Crystal Structure of an Asp-Substrate Peptide Bound to FIH—To investigate the structural basis of the FIH-catalyzed Asp hydroxylation, we attempted to co-crystallize wild type FIH with the Asp-substrate Peptide 2. However, initial attempts did not yield a structure of FIH in complex with the Asp-substrate peptide. Examination of the FIH-HIF1αCAD complex structure reveals an important hydrogen-bonding interaction between the HIF1αCAD substrate Asn amide and the side chain amide of Gln-239 of FIH (46). We hypothesized that the hydroxylated Asp residue binds in a similar manner but that the interaction is weaker due to the acidity of the aspartate side chain. Therefore, we produced a FIH variant in which Gln-239 is substituted with a histidine residue and showed that it also displays aspartate hydroxylase activity against Peptide 2 (supplemental Fig. S36). Co-crystallization of FIH Q239H with Peptide 2 led to a structure for FIH Q239H in complex with Zn(II), *N*-oxalylglycine (NOG), and the substrate peptide at the enzyme active site (refined to 2.2 Å resolution, supplemental Table 1). Except for the N-terminal 15 residues, the overall FIH Q239H structure is very similar to that reported for wt FIH (root mean square deviation for $\text{C}\alpha$ 0.22 Å, PDB ID 1H2K). The substrate Asp residue in Peptide

2 appears to be positioned at the FIH Q239H active site by hydrogen bonds to His-239 and neighboring Arg-238, in a similar manner as Asn-803 in the HIF1αCAD and Asn-1945 in the Notch 1 substrate peptides (Fig. 7). Overall, although we cannot be certain that wild type FIH binds Asp residues in the same manner as FIH Q239H, the observations suggest that it is likely that the FIH-catalyzed Asp hydroxylation also forms the 2*S*,3*S*-hydroxylated product (supplemental Scheme S2).

DISCUSSION

AnkyrinR is considered a “structural” protein that functions as an adapter linking the spectrin-based cytoskeleton to the erythrocyte membrane by interaction with spectrin and a range of integral membrane proteins including the anion exchanger (19). Our combined results arising from studies with synthetic peptides and recombinant protein purified from bacteria and human cells as well as endogenous protein purified from mice and a human, provide evidence that the membrane binding domain of ankyrinR is subject to multiple FIH-catalyzed hydroxylations. FIH is conserved in mammals, which implies that the multiple hydroxylations that we have identified are likely to be conserved in ankyrinR (supplemental Fig. S29). The results also indicate that other cytoskeletal

ankyrins are likely to be hydroxylated by FIH both at Asn and, possibly, Asp residues.

Analyses of the identified hydroxylation sites of D34 in light of a crystal structure (29) reveals that the hydroxylated Asn and Asp residues are dispersed across the convex surface of D34 (supplemental Fig. S37). Evidence for the importance of the sequence of individual ARs in determining substrate selectivity comes from the lower levels of hydroxylation for Asn residues with a prolyl residue at the -1 position relative to the target Asn residue (Table 1). However, although the presence of a -1 prolyl residue appears to block hydroxylation in 18-residue peptides, there was clear evidence for Asn hydroxylation at Asn-431 (present in a SPNV motif) and Asn-761 (present in a SPNE motif) in recombinant D34, demonstrating that, at least within the context of ARD proteins, FIH can be very tolerant of the residues within individual ARs.

The observation that FIH can catalyze the hydroxylation of Asp residues at the same conserved hydroxylation position as observed for Asn hydroxylations significantly expands the potential scope of FIH-catalyzed hydroxylations *in vivo*. The fact that we observed FIH-catalyzed Asp hydroxylation both in ankyrinR and ankyrinB suggests that this modification may occur in multiple proteins, although the available evidence suggests that it is less prevalent than Asn hydroxylation. Indeed, in ARDs aspartate is the second most common residue at the target hydroxylation position after asparagine (supplemental Fig. S32), suggesting that FIH-catalyzed Asp hydroxylation of ARDs could be common. Previous studies on the selectivity of FIH with respect to hydroxylation of the HIF-1 α C-terminal transcriptional activation domain have found that substitution of an Asp residue for the hydroxylated Asn residue (Asn-803) does not allow for hydroxylation (3), at least with a peptide fragment of HIF-1 α . Consistent with this, we did not observe hydroxylation of the 18-residue D34 peptide fragment containing Asp-695 despite clear evidence for hydroxylation at this site within the ARD. The collected results support the proposal that both the sequence of individual ankyrin repeats and secondary/tertiary structure considerations play roles in determining whether particular Asn or Asp residues in an ARD protein are substrates for FIH.

Another 2OG oxygenase, the epidermal growth factor (EGF) Asp/Asn hydroxylase (β -Asp/Asn hydroxylase (AspH or BAH)) has been found to catalyze β -hydroxylation of both Asp and Asn residues in EGF-like domains (47, 48). This enzyme produces hydroxy-Asp/Asn residues with the 2*S*, 3*R*-stereochemistry (49). In contrast, FIH produces β -hydroxyasparagine residues with the 2*S*, 3*S*-stereochemistry (45). NMR analysis of a hydroxylated Asp-substrate peptide indicates that hydroxylation occurs at the β -carbon position of the target Asp residue. Crystallographic analyses with the FIH Q239H variant demonstrate that the hydroxylated Asp residue adopts a similar conformation at the FIH active site as the hydroxylated Asn residue in ARDs and in HIF-1 α CAD, supporting the proposal that FIH catalyzes 3*S*-hydroxylation of Asp residues. 3*S*-Hydroxylation of aspartic acid has not been previously identified as a post-translational modification.

The observation that FIH-catalyzed hydroxylation of D34 results in stabilization of its conformation supports the pro-

posal based on work with consensus ARD proteins (17, 18) that Asn hydroxylation stabilizes the ARD folds of naturally occurring proteins. The combined crystallographic (17), NMR (18) and CD/DSC analyses reveal that hydroxylation does not change the stereotypical ARD-fold but causes stabilization via a process involving formation of a new hydrogen bond with the side chain of the residue at the -2 position relative to the hydroxylated asparagine. In all but one of the ankyrinR/D34 Asn residues observed to be hydroxylated by FIH, an appropriate residue at the -2 position for hydrogen bonding with the introduced alcohol was present. The exception (Asn-464) is present in a KVN sequence and was observed to be hydroxylated to a high level in recombinant D34, although we were unable to determine whether this site is hydroxylated *in vivo* due to limitations of the proteomic analyses. Thus, it is reasonable to propose that the stabilizing effect of hydroxylation on D34 results from the same mechanism proposed for the consensus ARD-proteins. However, for the consensus ARD proteins the hydroxylation occurred to a high level (>90%) at one or two sites. In contrast, it is likely that the hydroxylation-induced stabilization observed for D34, at least *in vitro*, results from multiple hydroxylations. These results raise the possibility of ankyrin repeat hydroxylation not only regulating the structure of localized region of ARD proteins and, hence, protein-protein interactions involving specific regions but of multiple hydroxylations "fine-tuning" the overall biophysical properties of ARD-proteins, including the spring-like behavior of some ARDs, a property proposed to be associated with mechano-transduction (30, 50).

Hydroxylation of ARD proteins has been previously shown to weaken their protein-protein interactions with FIH (6), a property that may regulate the amount of FIH available to hydroxylate HIF- α . To test whether the multiple incomplete hydroxylations observed for ankyrinR have the potential to modify a known protein-protein interaction, we investigated the effect of FIH-catalyzed hydroxylation on the binding of D34 and D12 regions to band 3. Treatment with FIH (but not a catalytically inactive variant) reduced the binding of D34, but not D12, to CBD3. Interestingly, these observations suggest that the consequences of AR hydroxylation within subdomains of the same ARD can be different. Together with experimental analyses (43), structural models for the interaction of ankyrinR with CDB3 tetramer (29) imply that the D34 region is more important for binding than the D12 region. It is possible that FIH-catalyzed multiple hydroxylations of D34 have a greater effect on CDB3 binding than that of D12, at least in part because the D34 hydroxylation sites make closer contact with CDB3. Although the physiological significance of the observed reduction in CBD3 binding to hydroxylated D34, if any, is unclear, the results demonstrate the potential for multiple, but incomplete, ARD hydroxylations to modulate protein-protein interactions. In this regard, it is also of interest that recent work has shown that the extent of folding of the ARD protein I κ B α regulates its binding to the transcriptional activator nuclear factor κ B (51, 52).

Acknowledgments—We are grateful to M. Nutley for contributions to the DSC experiments and B. Novák and J. S. O. McCullagh for encouragement.

REFERENCES

- Mahon, P. C., Hirota, K., and Semenza, G. L. (2001) *Genes. Dev.* **15**, 2675–2686
- Lando, D., Peet, D. J., Whelan, D. A., Gorman, J. J., and Whitelaw, M. L. (2002) *Science* **295**, 858–861
- Hewitson, K. S., McNeill, L. A., Riordan, M. V., Tian, Y. M., Bullock, A. N., Welford, R. W., Elkins, J. M., Oldham, N. J., Bhattacharya, S., Gleadle, J. M., Ratcliffe, P. J., Pugh, C. W., and Schofield, C. J. (2002) *J. Biol. Chem.* **277**, 26351–26355
- Lando, D., Peet, D. J., Gorman, J. J., Whelan, D. A., Whitelaw, M. L., and Bruick, R. K. (2002) *Genes. Dev.* **16**, 1466–1471
- Cockman, M. E., Lancaster, D. E., Stolze, I. P., Hewitson, K. S., McDonough, M. A., Coleman, M. L., Coles, C. H., Yu, X., Hay, R. T., Ley, S. C., Pugh, C. W., Oldham, N. J., Masson, N., Schofield, C. J., and Ratcliffe, P. J. (2006) *Proc. Natl. Acad. Sci. U.S.A.* **103**, 14767–14772
- Coleman, M. L., McDonough, M. A., Hewitson, K. S., Coles, C., Mecnovic, J., Edelmann, M., Cook, K. M., Cockman, M. E., Lancaster, D. E., Kessler, B. M., Oldham, N. J., Ratcliffe, P. J., and Schofield, C. J. (2007) *J. Biol. Chem.* **282**, 24027–24038
- Ferguson, J. E., 3rd, Wu, Y., Smith, K., Charles, P., Powers, K., Wang, H., and Patterson, C. (2007) *Mol. Cell. Biol.* **27**, 6407–6419
- Cockman, M. E., Webb, J. D., Kramer, H. B., Kessler, B. M., and Ratcliffe, P. J. (2009) *Mol. Cell. Proteomics* **8**, 535–546
- Webb, J. D., Murányi, A., Pugh, C. W., Ratcliffe, P. J., and Coleman, M. L. (2009) *Biochem. J.* **420**, 327–333
- Cockman, M. E., Webb, J. D., and Ratcliffe, P. J. (2009) *Ann. N.Y. Acad. Sci.* **1177**, 9–18
- Mosavi, L. K., Cammett, T. J., Desrosiers, D. C., and Peng, Z. Y. (2004) *Protein Sci.* **13**, 1435–1448
- Schultz, J., Milpetz, F., Bork, P., and Ponting, C. P. (1998) *Proc. Natl. Acad. Sci. U.S.A.* **95**, 5857–5864
- Michaely, P., and Bennett, V. (1992) *Trends Cell Biol.* **2**, 127–129
- Bork, P. (1993) *Proteins* **17**, 363–374
- Myllyharju, J., and Kivirikko, K. I. (2001) *Ann. Med.* **33**, 7–21
- Myllyharju, J. (2003) *Matrix Biol.* **22**, 15–24
- Kelly, L., McDonough, M. A., Coleman, M. L., Ratcliffe, P. J., and Schofield, C. J. (2009) *Mol. Biosyst.* **5**, 52–58
- Hardy, A. P., Prokes, I., Kelly, L., Campbell, I. D., and Schofield, C. J. (2009) *J. Mol. Biol.* **392**, 994–1006
- Bennett, V., and Baines, A. J. (2001) *Physiol. Rev.* **81**, 1353–1392
- Ding, Y., Jiang, W., Su, Y., Zhou, H., and Zhang, Z. (2004) *Protein Expr. Purif.* **34**, 167–175
- Su, Y., Ding, Y., Jiang, W., Hu, X., and Zhang, Z. (2006) *Mol. Cell. Biochem.* **289**, 159–166
- Bennett, V., and Stenbuck, P. J. (1980) *J. Biol. Chem.* **255**, 2540–2548
- Werbeck, N. D., and Itzhaki, L. S. (2007) *Proc. Natl. Acad. Sci. U.S.A.* **104**, 7863–7868
- Otwinowski, Z., and Minor, W. (1997) *Methods Enzymol.* **276**, 307–326
- Brünger, A. T., Adams, P. D., Clore, G. M., DeLano, W. L., Gros, P., Grosse-Kunstleve, R. W., Jiang, J. S., Kuszewski, J., Nilges, M., Pannu, N. S., Read, R. J., Rice, L. M., Simonson, T., and Warren, G. L. (1998) *Acta Crystallogr. D Biol. Crystallogr.* **54**, 905–921
- Emsley, P., and Cowtan, K. (2004) *Acta Crystallogr. D Biol. Crystallogr.* **60**, 2126–2132
- Laskowski, R. A., MacArthur, M. W., Moss, D. S., and Thornton, J. M. (1993) *J. Appl. Crystallogr.* **26**, 283–291
- Painter, J., and Merritt, E. A. (2006) *Acta Crystallogr. D Biol. Crystallogr.* **62**, 439–450
- Michaely, P., Tomchick, D. R., Machius, M., and Anderson, R. G. (2002) *EMBO J.* **21**, 6387–6396
- Lee, G., Abdi, K., Jiang, Y., Michaely, P., Bennett, V., and Marszalek, P. E. (2006) *Nature* **440**, 246–249
- Costas, M., Mehn, M. P., Jensen, M. P., and Que, L., Jr. (2004) *Chem. Rev.* **104**, 939–986
- Ozer, A., and Bruick, R. K. (2007) *Nat. Chem. Biol.* **3**, 144–153
- Flashman, E., Davies, S. L., Yeoh, K. K., and Schofield, C. J. (2010) *Biochem. J.* **427**, 135–142
- Hewitson, K. S., Holmes, S. L., Ehrismann, D., Hardy, A. P., Chowdhury, R., Schofield, C. J., and McDonough, M. A. (2008) *J. Biol. Chem.* **283**, 25971–25978
- Previero, A., Coletti-Previero, M. A., and Jollès, P. (1967) *J. Mol. Biol.* **24**, 261–268
- Kuroda, M., Sakiyama, F., and Narita, K. (1975) *J. Biochem.* **78**, 641–651
- Finley, E. L., Dillon, J., Crouch, R. K., and Schey, K. L. (1998) *Protein Sci.* **7**, 2391–2397
- Taylor, S. W., Fahy, E., Murray, J., Capaldi, R. A., and Ghosh, S. S. (2003) *J. Biol. Chem.* **278**, 19587–19590
- Bienvenu, W. V., Déon, C., Pasquarello, C., Campbell, J. M., Sanchez, J. C., Vestal, M. L., and Hochstrasser, D. F. (2002) *Proteomics* **2**, 868–876
- Anderson, L. B., Maderia, M., Ouellette, A. J., Putnam-Evans, C., Higgins, L., Krick, T., MacCoss, M. J., Lim, H., Yates, J. R., 3rd, and Barry, B. A. (2002) *Proc. Natl. Acad. Sci. U.S.A.* **99**, 14676–14681
- Michaely, P., and Bennett, V. (1995) *J. Biol. Chem.* **270**, 22050–22057
- Davis, L., Lux, S. E., and Bennett, V. (1989) *J. Biol. Chem.* **264**, 9665–9672
- Chang, S. H., and Low, P. S. (2003) *J. Biol. Chem.* **278**, 6879–6884
- Binz, H. K., Stumpp, M. T., Forrer, P., Amstutz, P., and Plückthun, A. (2003) *J. Mol. Biol.* **332**, 489–503
- McNeill, L. A., Hewitson, K. S., Claridge, T. D., Seibel, J. F., Horsfall, L. E., and Schofield, C. J. (2002) *Biochem. J.* **367**, 571–575
- Elkins, J. M., Hewitson, K. S., McNeill, L. A., Seibel, J. F., Schlemminger, I., Pugh, C. W., Ratcliffe, P. J., and Schofield, C. J. (2003) *J. Biol. Chem.* **278**, 1802–1806
- Stenflo, J., Holme, E., Lindstedt, S., Chandramouli, N., Huang, L. H., Tam, J. P., and Merrifield, R. B. (1989) *Proc. Natl. Acad. Sci. U.S.A.* **86**, 444–447
- Stenflo, J. (1991) *Blood* **78**, 1637–1651
- Przywiecki, C. T., Staggers, J. E., Ramjit, H. G., Musson, D. G., Stern, A. M., Bennett, C. D., and Friedman, P. A. (1987) *Proc. Natl. Acad. Sci. U.S.A.* **84**, 7856–7860
- Kim, M., Abdi, K., Lee, G., Rabbi, M., Lee, W., Yang, M., Schofield, C. J., Bennett, V., and Marszalek, P. E. (2010) *Biophys. J.* **98**, 3086–3092
- Truhlar, S. M., Mathes, E., Cervantes, C. F., Ghosh, G., and Komives, E. A. (2008) *J. Mol. Biol.* **380**, 67–82
- Sue, S. C., Cervantes, C., Komives, E. A., and Dyson, H. J. (2008) *J. Mol. Biol.* **380**, 917–931
- Neidig, M. L., Brown, C. D., Light, K. M., Fujimori, D. G., Nolan, E. M., Price, J. C., Barr, E. W., Bollinger, J. M., Jr., Krebs, C., Walsh, C. T., and Solomon, E. I. (2007) *J. Am. Chem. Soc.* **129**, 14224–14231